Research Square

Preprints are preliminary reports that have not undergone peer review.
They should not be considered conclusive, used to inform clinical practice,
or referenced by the media as validated information.

Iodinated Heptamethinecyanine Dye / Dextran-Polyacrylamide Polymer / Gold Nanorods Nanohybrid with Plasmon Enhanced NIR Optical Response for Potential Bioimaging and Biosensing Applications

Oleg Yeshchenko

oleg.yeshchenko@knu.ua

Taras Shevchenko National University of Kyiv https://orcid.org/0000-0001-8927-5673

Oles Fedotov

Taras Shevchenko National University of Kyiv https://orcid.org/0009-0003-9401-9078

Pavlo Khort

Taras Shevchenko National University of Kyiv https://orcid.org/0000-0002-1169-2431

Dmytro Kobzev

Institute for Single Crystals https://orcid.org/0000-0002-7731-6420

Anatoliy Tatarets

Institute for Single Crystals https://orcid.org/0000-0003-4406-7883

Mykola Ischenko

Taras Shevchenko National University of Kyiv https://orcid.org/0000-0002-0851-1679

Volodymyr Doroschuk

Taras Shevchenko National University of Kyiv https://orcid.org/0000-0001-6703-1926

Pavlo Virych

Taras Shevchenko National University of Kyiv https://orcid.org/0000-0002-1463-1992

Natalia Kutsevol

Taras Shevchenko National University of Kyiv https://orcid.org/0000-0002-1468-4111

Research Article

Keywords: NIR cyanine dyes, Gold nanorods, Star-like polymer, Polyacrylamide, Metal-enhanced fluorescence, SERS, Bioimaging, Biosensing

Posted Date: November 25th, 2026

DOI: https://doi.org/10.21203/rs.3.rs-11857424/v1

License: This work is licensed under a Creative Commons Attribution 4.0 International License.
Read Full License

Additional Declarations: The authors declare no competing interests.

Iodinated Heptamethinecyanine Dye / Dextran-Polyacrylamide Polymer / Gold Nanorods Nanohybrid with Plasmon Enhanced NIR Optical Response for Potential Bioimaging and Biosensing Applications

Oleg Yeshchenko,[1*] Oles Fedotov,[1] Pavlo Khort,[1] Dmytro Kobzev,[2] Anatoliy Tatarets,[2] Mykola Ischenko,[3] Volodymyr Doroschuk,[3] Pavlo Virych,[3] Natalia Kutsevol[3]

[1] *Faculty of Physics, Taras Shevchenko National University of Kyiv, Kyiv, Ukraine*

[2] *Institute of Functional Materials Chemistry, State Scientific Institution "Institute for Single Crystals" of National Academy of Sciences of Ukraine, Kharkiv, Ukraine*

[3] *Faculty of Chemistry, Taras Shevchenko National University of Kyiv, Kyiv, Ukraine*

Abstract

Multifunctional hybrid nanoplatforms operating within the near-infrared (NIR) biological transparency window hold immense potential for various biomedical applications. In this work, we report the synthesis and optical investigation of water-soluble 3-component nanohybrids based on iodinated heptamethine cyanine dyes (2I-HITC and 4I-HITC), a star-like dextran-graft-polyacrylamide copolymer matrix (D6-PAA), and plasmonic gold nanorods (AuNRs) with longitudinal surface plasmon resonance (LSPR) at 660 nm (AuNR660) and 745 nm (AuNR745). The D6-PAA polymer matrix effectively reduces hydrophobic dye aggregation as well as encapsulates dye molecules and AuNRs. Spectral tuning of the LSPR of AuNRs to match the NIR absorption and emission bands of the dyes led to strong plasmon-enhanced photoluminescence (SEPL) and Raman scattering (SERS). The optical response exhibited a non-monotonic concentration dependence dictated by the competition between plasmonic enhancement and non-radiative Förster resonance energy transfer (FRET) quenching. Due to weaker FRET quenching and stronger local electromagnetic field hot spots, the 2I-HITC/D6-PAA/AuNR745 nanohybrid achieved the highest enhancement factors for both PL (26.8-fold) and SERS (25.4-fold under 785 nm excitation). Theoretical calculations using Boyd's local-field enhancement model strongly corroborated the experimental SERS results, confirming the spatial proximity of the functional components within the polymer matrix. These findings highlight the three-component 2I-HITC/D6-PAA/AuNR745 nanohybrid as a potential platform for high-sensitivity NIR fluorescence bioimaging and diagnostic SERS sensing.

Keywords: NIR cyanine dyes; Gold nanorods; Star-like polymer; Polyacrylamide; Metal-enhanced fluorescence; SERS; Bioimaging; Biosensing

Introduction

Recently, optical and, in particular, fluorescent, research methods in biology and medicine have become widely used, as well as their use in clinical diagnostics. As the main elements in any fluorescent research method, fluorescent compounds (primarily, organic dyes) have long been used for diagnostic purposes. However, with the development of personalized medicine, focused on the study of living cells and whole organisms *in vivo*, the idea of using fluorescent dyes not only for imaging but also for therapeutic purposes has emerged, giving rise to their application in theranostics [1–4].

To obtain a fluorescent signal and/or therapeutic effect from such molecules, they must effectively absorb light in the desired spectral range. It should be noted that only light in the near-infrared (NIR) range (600–900 nm: biological transparency window) is poorly absorbed by biological macromolecules, water, and other components of biological objects, and therefore has a very weak influence on the processes occurring in the body [5,6]. In this spectral range, the light absorption and scattering by major endogenous chromophores (such as water, hemoglobin, and melanin) are minimized, thereby enabling maximum optical penetration into biological tissues without inducing thermal damage [7,8]. It is clear that such restrictions on the spectral range of fluorescent dyes significantly reduce the possibility of their selection. In addition, a fluorescent dye or dye-based nanomaterial for biological and medical applications must have a high extinction coefficient and fluorescence quantum yield, sufficient solubility in water, and acceptable photostability and chemical stability.

Cyanines are a highly promising class of dyes due to the significant flexibility of their spectral, photophysical, and photochemical properties [9,10]. Heptamethine cyanine dyes have very low phototoxicity and fit well into the NIR optical window, making them widely used in diagnostics. For example, indocyanine green (ICG) is used for *in vivo* imaging and fluorescence-guided surgery [11,12]. In addition to their use as fluorescent markers, heptamethine cyanine dyes can also be used as photosensitizers in photodynamic therapy (PDT) [13–16] and in IR photoimmunotherapy [17]. However, their relatively low cytotoxicity limits their therapeutic efficacy. One strategy to overcome this limitation is the encapsulation of cyanine dyes into nanoparticles. For example, nanoparticle formulations of indocyanine green (ICG) have demonstrated considerable potential for combined diagnostic imaging, drug delivery, and photodynamic therapy of solid tumors [18]. Another approach to enhance the cytotoxicity of these dyes is to incorporate heavy atoms, such as iodine, into the dye structure thereby promoting intersystem crossing through the heavy atom effect [19–21]. To the best of our knowledge, however, the spectral and photophysical properties of nanoparticle formulations of iodinated cyanine dyes have not yet been investigated.

Among the diverse array of inorganic nanomaterials, noble metal plasmonic nanoparticles (specifically gold nanorods, AuNRs) have attracted significant research interest due to their unique optical properties, chemical stability, and highly versatile surface chemistry [22,23]. Unlike spherical nanoparticles, AuNRs exhibit two distinct localized surface plasmon resonance (LSPR) bands: transverse and longitudinal [24]. By precisely adjusting the aspect ratio (length-to-diameter ratio) of the nanorods, the longitudinal LSPR wavelength can be tuned effectively into the NIR region (650–1100 nm) [25,26]. A foundational advantage of AuNRs in diagnostic and therapeutic applications is their ability to act as effective nanoantennas that locally enhance the

electromagnetic field in the immediate vicinity of their surface [27,28]. When NIR fluorescent dyes or photosensitizers are positioned at a controlled distance from the gold core, metal-enhanced fluorescence (MEF) occurs [29,30]. This effect substantially enhances fluorescence emission signals, overcoming a major inherent limitation of organic NIR fluorophores – their relatively low quantum yield [31,32]. Concurrently with fluorescence enhancement, the localized electromagnetic field generated by the nanorods intensifies intersystem crossing in immobilized dye molecules [33]. This leads to a marked increase in the efficiency of reactive oxygen species (ROS) generation, particularly singlet oxygen ($^1O_2$), which is crucial for enhancing the efficacy of photodynamic therapy (PDT) [34,35].

Despite their significant potential, the direct *in vivo* application of free AuNRs is severely hindered by the cytotoxicity of surfactants (such as cetyltrimethylammonium bromide, CTAB) used during their seed-mediated synthesis, as well as the tendency of free nanoparticles to undergo rapid aggregation and opsonization in physiological media [36,37]. To resolve these limitations, the surface of AuNRs is functionalized with dedicated polymer shells to form nanohybrid complexes [38]. The polymeric coating fulfills several key functions: it mitigates cytotoxicity by shielding residual CTAB, provides steric stabilization in the bloodstream, and serves as a versatile matrix for covalent or non-covalent conjugation of NIR dyes [39].

Among various polymeric materials used for nanohybrid engineering, polyacrylamide (PAA) and its branched or star-like architectural variants are of particular scientific interest [40]. Linear PAA features high hydrophilicity, chemical inertness, and a high density of amide groups ($–CONH_2$), forming swollen three-dimensional networks around metallic nanoparticles [41]. However, advanced theranostic systems increasingly rely on star-like copolymer architectures, notably macromolecular matrices comprising a biocompatible dextran core with grafted polyacrylamide side chains (Dextran-graft-PAA) [42–44]. The branched, star-like structure provides a significantly higher local concentration of functional groups within a compact spatial volume compared to linear analogs [40,45]. The central dextran core imparts enhanced biocompatibility, while the dense, flexible PAA grafts allow for the precise spatial encapsulation of both metal nanoparticles and photosensitizers [46–48]. This specialized molecular layout ensures optimal photosensitizer-to-plasmonic nanoparticle distance that provides enhancement of ROS generation and corresponding high antitumor and antibacterial photodynamic efficiency [46–48].

Consequently, the design and investigation of plasmonic nanohybrids based on gold nanorods coated with star-like dextran-graft-polyacrylamide copolymers and functionalized with NIR dyes represent a highly promising strategy in modern theranostics. This integrated architecture allows the seamless combination of ultra-sensitive optical imaging in the biological transparency window with high-efficiency photodynamic and photothermal therapies against malignant neoplasms.

In this work, we developed the water-soluble NIR dye/polymer/metal nanoparticle 3-component nanohybrids with plasmon-enhanced optical response in the near-IR range for potential biomedical applications. As respective functional components of the nanohybrid we use a 1, iodinated heptamethine cyanines (2I-HITC and 4I-HITC comprising 2 and 4 iodine atoms, respectively) as the NIR-fluorescent component, Dextran-grafted-PAA as a matrix polymer component, and AuNRs as a plasmonic component. The high plasmon enhanced photoluminescence and SERS response of NIR-dyes in the 2I(4I)-HITC/D-PAA/AuNR

nanohybrids was revealed indicating the high potential of this nanohybrid for application in NIR optical bioimaging and diagnostic SERS sensing.

Experimental

2I-HITC and 4I-HITC dyes synthesis

Starting materials and solvents were purchased from *Sigma-Aldrich*. 5-Iodo-1,2,3,3-tetramethyl-3*H*-indol-1-ium iodide, 4,6-diiodo-1,2,3,3-tetramethyl-3*H*-indol-1-ium iodide and iodinated heptamethine cyanine dyes (2I-HITC and 4I-HITC) were obtained according to [19]. ^{1}H-NMR and ^{13}C-NMR spectra were recorded on a Bruker Avance III HD (^{1}H at 400 MHz and ^{13}C at 101 MHz) spectrometer and a BBO probe equipped with a Z gradient coil. ^{1}H-NMR and ^{13}C-NMR spectra were measured in DMSO-d_6 at 25 °C. HRMS spectra were obtained using a Xevo G2-XS QTOF device. The samples were injected direct to MS using MeOH as a solvent. Data was acquired using resolution mode under positive electrospray ionization. Capillary voltage was 2.0 kV. Cone voltage was 40 V. Scan times were 0.5 s.

5-Iodo-2-((1,3,5,7)-7-(5-iodo-1,3,3-trimethylindolin-2-ylidene)hepta-1,3,5-trien-1-yl)-1,3,3-trimethyl-3H-indol-1-ium iodide (2I-HITC)

5-Iodo-1,2,3,3-tetramethyl-3*H*-indol-1-ium iodide (300 mg, 0.70 mmol) and N-[5-(phenylamino)-2,4-pentadienylidene]aniline hydrochloride (100.0 mg, 0.35 mmol) were dissolved in 8 mL of acetic anhydride and heated at 90–100 °C during 10 min. Then, the reaction mixture was cooled to 50 °C, following by the addition of pyridine (3 mL) and heating at 90–100 °C during 5 min, resulting in the formation of the product. Then, the reaction mixture was cooled to r.t. during 10 min. The desired dye was precipitated with ether, filtered off and washed with ether. The crude product was column purified on Silica gel 60 using 1–20% methanol-chloroform as eluent. Fraction with the dye was collected, evaporated, washed with ether and vacuum-dried. Yield: 138 mg (50%) as a dark blue metallic powder, R_f 0.54 (Silica gel 60, $CHCl_3$: MeOH : CH_3COOH = 4 : 2 : 0.14, v/v/v). ^{1}H-NMR (400 MHz, DMSO-d_6), δ, ppm: 7.96 (2H, s, CH, arom.), 7.86 (2H, t, J = 13.2 Hz, CH), 7.76 (1H, t, J = 12.6 Hz, CH), 7.73 (2H, d, J = 8.2 Hz, CH, arom.), 7.19 (2H, d, J = 8.3 Hz, CH, arom.), 6.54 (2H, t, J = 12.6 Hz, CH), 6.30 (2H, d, J = 13.7 Hz, CH), 3.54 (6H, s, N-CH_3), 1.62 (12H, s, $(CH_3)_2$). ^{13}C-NMR (100 MHz, DMSO-d_6), δ, ppm: 171.05, 156.28, 150.93, 143.33, 142.80, 136.90, 130.99, 125.79, 113.12, 104.22, 88.72, 48.60, 31.18, 26.83. HRMS: m/z (ESI^+) $C_{29}H_{31}I_2N_2^+$ calculated $[M]^+$ 661.0577, found m/z: 661.0576.

4,6-Diiodo-2-((1,3,5,7)-7-(4,6-diiodo-1,3,3-trimethylindolin-2-ylidene)hepta-1,3,5-trien-1-yl)-1,3,3-trimethyl-3H-indol-1-ium iodide (4I-HITC)

The mixture of 4,6-diiodo-1,2,3,3-tetramethyl-3*H*-indol-1-ium iodide (110 mg, 0.20 mmol) and N-[5-(phenylamino)-2,4-pentadienylidene]aniline hydrochloride (28.3 mg, 0.1 mmol) was dissolved in 4 mL of acetic anhydride and heated at 90–100 °C during 10 min. Then, the reaction mixture was cooled to 50 °C, following by the addition of pyridine (3 mL) and heating at 90–100 °C during 5 min, resulting in the formation of the product. Then, the reaction mass was cooled to r.t. The desired dye was precipitated with ether, filtered off and washed with ether. The crude product was column purified on Silica gel 60 using 1–20% methanol-chloroform as eluent. Fraction with the dye was collected, evaporated, washed with ether and vacuum-dried. Yield: 74 mg (55%) as a dark blue metallic powder; R_f 0.56 (Silica gel 60, $CHCl_3$: MeOH : CH_3COOH = 4 : 2 : 0.14, v/v/v). ^{1}H-NMR (400 MHz, DMSO-d_6), δ, ppm: 7.94 (2H, s, CH, arom.), 7.91 (2H, t, J = 13.3 Hz, CH), 7.80 (2H, s, CH, arom.), 7.76 (1H, t, J = 13.5 Hz, CH), 6.59 (2H, t, J = 12.6 Hz,

CH), 6.33 (2H, d, J = 13.8 Hz, CH), 3.53 (6H, s, N-CH_3), 1.72 (12H, s, $(CH_3)_2$). ^{13}C-NMR (100 MHz, DMSO-d_6), δ, ppm: 171.34, 156.51, 150.92, 143.17, 142.28, 131.07, 125.50, 116.73, 112.70, 104.28, 91.60, 48.71, 31.24, 26.79. HRMS: m/z (ESI$^+$) $C_{29}H_{29}I_4N_2^+$ calculated $[M]^+$ 912.8510, found m/z: 912.8514.

Structure of heptamethine cyanines 2I-HITC and 4I-HITC is presented in Fig. 1.

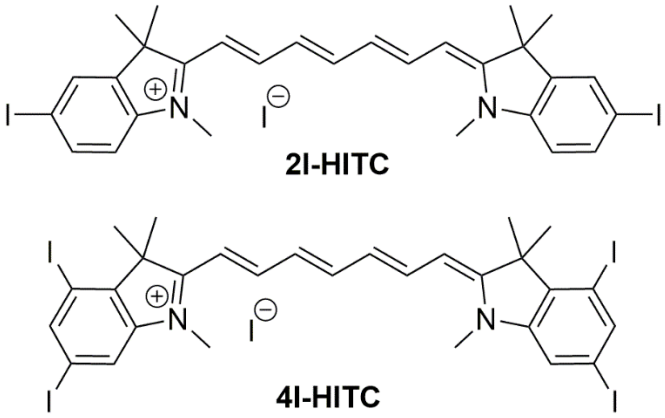


Fig. 1. Structure of heptamethine cyanines 2I-HITC and 4I-HITC

Polymer synthesis

Dextran with molecular weights Mw=6 ×10^3 g/mol (D6) was purchased from Sigma-Aldrich. Cerium (IV) ammonium nitrate from Sigma-Aldrich was used as initiator. Dextran samples and the ceric salts were used without further purification. Acrylamide (AA) was obtained from Reanal (Hungary), and was twice re-crystallized from chloroform.

Dextran-graft-Polyacrylamide copolymer. The Dextran-graft-Polyacrylamide copolymer was synthesized using a ceric ion-induced redox initiation method. This redox process generates free-radical sites exclusively on the polysaccharide backbone, thereby preventing the formation of polyacrylamide (PAA) homopolymer [45]. The resulting active radicals initiate the growth of PAA graft chains in the presence of the acrylamide monomer. The average number of grafting sites per dextran molecule depends on the molar ratio of ceric ions to dextran [13]. For the synthesis of the Dextran-graft-Polyacrylamide copolymer, a molar ratio of Ce(IV) to dextran (mol Ce(IV)/mol Dextran = 10), was used.

Dextran (1.67×10^{-4} mol) was dissolved in 20 mL of distilled water. The solution was stirred while argon was bubbled through it for 20 min to remove dissolved oxygen. A predetermined amount of the Ce(IV)/HNO_3 initiator (0.125 N HNO_3) was then added. Twenty minutes later, 1 g of acrylamide (AA) monomer was introduced, and the polymerization was allowed to proceed under an argon atmosphere for 24 h. At the end of the reaction, the copolymer was precipitated with an excess of acetone, redissolved in water, and freeze-dried. The obtained sample was designated as D6-PAA.

The copolymer was characterized by size-exclusion chromatography (SEC) using a multidetector system consisting of an LC-10AD Shimadzu pump (flow rate 0.5 mL/min), a WISP 717C automatic injector (Waters), three coupled 30 cm Shodex OH-pak columns (803HQ, 804HQ, and 806HQ), a DAWN F multi-angle light scattering (MALS) detector (Wyatt Technology), and an R410 differential refractive index detector (Waters). Distilled water containing 0.1 M $NaNO_3$

was used as the eluent. Polymer solutions for SEC analysis were prepared at a concentration of 3 g/L.

SEC equipped with multi-angle light scattering (LS) and differential refractive index (RI) detectors enables the determination of the weight-average molecular weight (Mw) and number-average molecular weight (Mn). A single intense, nearly symmetrical peak was observed in both the LS and RI detector signals, confirming the absence of polyacrylamide homopolymer in the synthesized D6-PAA copolymer. The molecular characteristics of the D6-PAA copolymer are summarized in Tab. 1. The high values of Mw and radius of gyration (Rz), together with the relatively low dextran content (Tab. 1), indicate that the synthesized copolymer possesses a star-shaped architecture.

The D6-PAA copolymer will subsequently be used as a matrix for nanosystems synthesis.

Table 1. Molecular parameter of D6-PAA

Sample	$M_w \times 10^{-6}$ $g \cdot mol^{-1}$	M_n	R_z, nm	M_w/M_n	w, % Dextran component
D6-PAA	1.093	0.640	76.5	1.69	0.55

Gold nanorods synthesis and D6-PAA/AuNRs preparation

Gold nanorods were synthesized using the technique described in Nikoobakht and El-Sayed [49]. All solutions were prepared using deionized water. Required amount of hexadecyltrimethylammonium bromide (CTAB, Merck) was heated to 35 °C until completely dissolved to prepare a 0.1 M solution. 1 mL of CTAB (0.1 M) was mixed with 25 μL of $HAuCl_4$ (0.5 mM, Merck), and stirred at 400 rpm for 10 min at 35 °C. 60 μL of 10 mM $NaBH_4$ (Merck) was added to the mixture and was incubated for 10 min to produce small non-plasmonic nanoparticles (AuNPs). To obtain AuNRs, 250 μL of 1 mM $HAuCl_4$ was added to 5 mL of 0.1 M CTAB. The mixture was stirred at 160 rpm, 35 °C for 10 min. Then, L-ascorbic acid (10 mM, Merck) was added dropwise until the solution was completely discolored. 120 μL of AuNPs solution was added immediately after ascorbic acid. The mixture was gently stirred at 160 rpm for 30 min. During this time, the color of the solution was changed from transparent to gray, which corresponds to AuNRs with an absorbance maximum of 745 nm (AuNR745 further in the text). Obtaining AuNRs with absorbance maxima of 660 nm (AuNR660 further in the text) was achieved by reducing the $HAuCl_4$ solution to 15 μL. The AuNRs solution was centrifuged 4 times in CTAB at 6000 rpm (5 min) (Hermle z216m, Wehingen, Germany) to remove spherical AuNPs. AuNRs were precipitated at 13,000 rpm (15 min). The precipitate was then re-dissolved in deionized water and re-precipitated under the same conditions. The manipulations were repeated 4 times to remove the remaining CTAB. After the last centrifugation, the sediment was transferred into a D6-PAA solution (1 mg/mL).

Gold concentration

An aliquot of the AuNRs in D6-PAA was taken to determine the amount of gold in stock solution. An aliquot of 0.200 mL of the sample was transferred into a 10.00 mL volumetric flask, followed by the addition of 1.0 mL of freshly prepared *aqua regia*. The mixture was allowed to stand for 20 min and was subsequently diluted to the mark with deionized water. The flame atomic absorption

determination of gold was performed using a SpectrAA 50 flame atomic absorption spectrometer (Varian Inc., Palo Alto, California, USA) under the following operating conditions: air–acetylene flame, lamp current of 7 mA, resonance line wavelength of 267.6 nm, and a spectral slit width of 1 nm. The expanded uncertainty with a coverage factor of k = 2 did not exceed 6%. Accordingly, the concentrations of gold and polymer in the stock solutions of D6-PAA/AuNRs were obtained as: 1 mg/mL (D6-PAA), 0.122 mg/mL (gold in D6-PAA/AuNR660), 0.141 mg/mL (gold in D6-PAA/AuNR745).

2-component 2I(4I)-HITC/D6-PAA and 3-component 2I(4I)-HITC/D6-PAA/AuNR nanohybrid aqueous solution preparation

To prepare the aqueous solution of 2I-HITC and 4I-HITC dye of desired concentration, the appropriate volumes of stock solution of dye in dimethyl sulfoxide (DMSO) and deionized water were mixed. To obtain 2-component 2I(4I)-HITC/D6-PAA or respectively 3-component 2I(4I)-HITC/D6-PAA/AuNR660 (2I(4I)-HITC/D6-PAA/AuNR745) nanohybrid aqueous solution with desired concentrations of components, the appropriate volumes of dye stock solution in DMSO and aqueous solution of D6-PAA or respectively D6-PAA/AuNR660 (D6-PAA/AuNR745) were mixed and diluted with deionized water. After mixing, the mixture was stirred for 5 min. Then, the absorption and photoluminescence (PL) spectra were monitored. About 45 min after mixing, the spectra entered a steady state, so further optical measurements were performed 1 h after mixing. The obtained aqueous solutions of both 2- and 3-component nanohybrids demonstrate good stability over time, namely, 1 week after mixing, the intensity of the absorption and PL spectra decreases by no more than 5%.

TEM

TEM analysis was performed using a Jeol JEM 1400 operating at 120 keV, equipped with a Gatan Orius digital camera. A 3 μL of the D6-PAA/AuNR colloids were placed onto a formvar-coated copper grid (without a carbon film) and left to air-dry at room temperature for 4 hours before imaging. 23 images were acquired and analyzed for each D6-PAA/AuNR660 and D6-PAA/AuNR745 nanohybrid.

Optical spectroscopy

Absorption spectra were measured by an Agilent Cary 60 spectrophotometer. PL spectra under 750 nm for 2I-HITC and 730 nm for 4I-HITC NIR excitation were measured by a Shimadzu RF-6000 spectrofluorophotometer. The absorption and PL measurements were performed using a quartz cuvette with a pathlength of 1 cm. Raman spectra were measured by a Renishaw RM1000 μ-Raman spectrometer under 532 and 785 nm laser excitations. The spectra were taken from a dried drop of the solution deposited on an Al substrate. All optical measurements were performed at room temperature. Measurements of absorption, photoluminescence, and Raman scattering spectra were replicated five times for each sample to verify data reproducibility.

Since the PL spectra and the absorption spectra of dyes and AuNRs overlap strongly, significant reabsorption of exciting and emitted (PL) photons would occur. Therefore, to take into account the reabsorption, the PL intensity at the wavelength λ_{pl} was defined as

$I\left(\lambda_{pl}\right) = I_{measur}\left(\lambda_{pl}\right) \cdot 10^{\left[\Delta D(\lambda_{exc}) + \Delta D(\lambda_{pl})\right]}$, where λ_{exc} is the excitation wavelength, $I_{measur}\left(\lambda_{pl}\right)$ is the measured PL intensity at the wavelength λ_{pl}; $\Delta D(\lambda) = D_{hybr}(\lambda) - D_{dye}(\lambda)$ is the difference of optical densities of hybrid and free dye at the wavelength λ.

RESULTS AND DISCUSSION

TEM characterization

D6-PAA/AuNR nanohybrids were synthesized via the procedure described above. The TEM characterization was performed to establish morphology and dimensional characteristics of the nanohybrids. TEM analysis confirmed the formation of AuNRs with different length and aspect ratio. The typical TEM images of the samples containing the AuNRs of two different types are presented in Fig. 2. TEM revealed that D6-PAA/AuNR660 nanohybrid contains the NRs of (26.4 ± 5.3) nm in length and (9.2 ± 1.6) nm in diameter (aspect ratio R = 2.9); D6-PAA/AuNR745 nanohybrid contains the NRs of (34.5 ± 8.3 nm) in length and (9.3 ± 1.7) nm in diameter (aspect ratio R = 3.7). The AuNRs in different nanohybrids have the same diameter and differ by the length. AuNRs are characterized by quite narrow size distributions by both diameter and length.

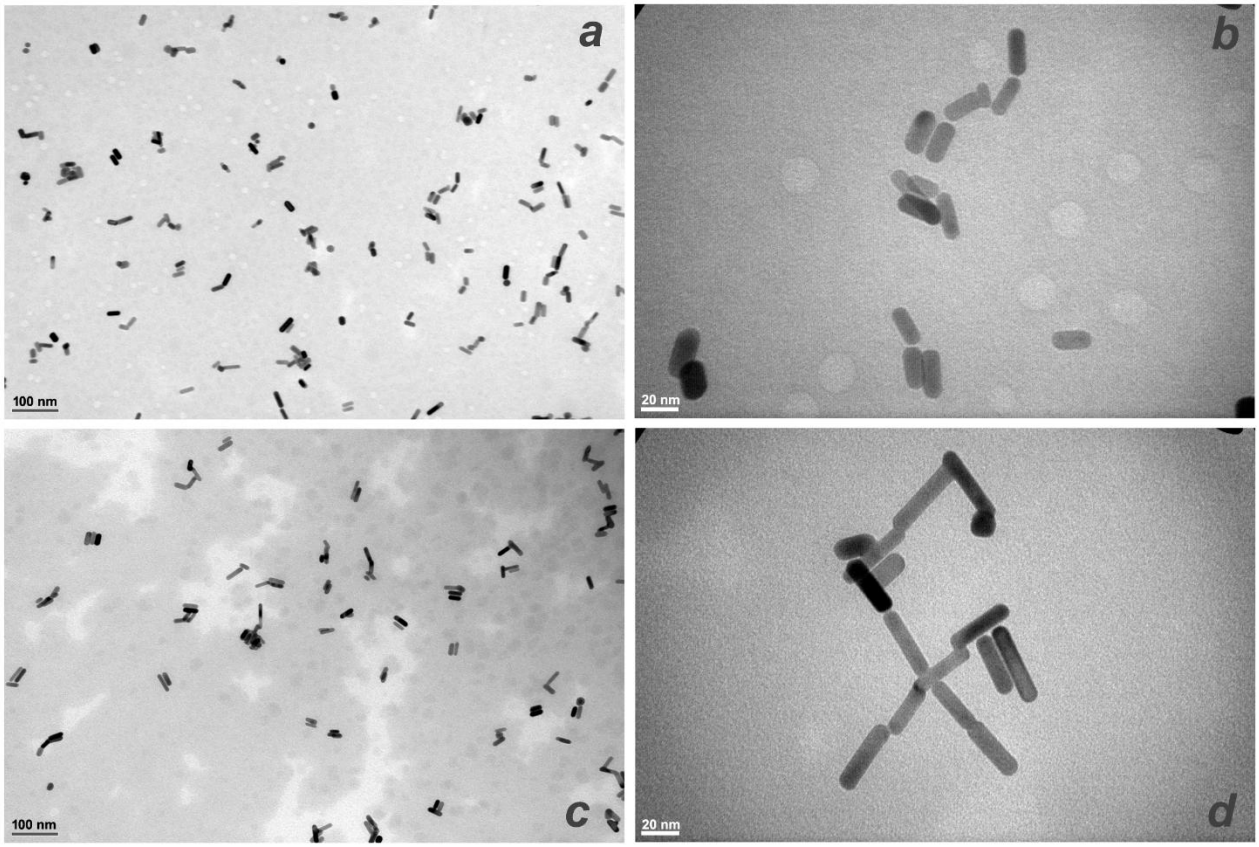


Fig. 2. Typical TEM images of AuNRs in D6-PAA/AuNR660 nanohybrid (a,b) and in D6-PAA/AuNR745 nanohybrid (c,d).

The TEM images show that the nanorods are not distributed uniformly in space, but are collected in groups, which indicates the fact of their entry into the volume of polymer

macromolecules and binding to them, resulting in the formation of metal-polymer nanohybrids. Although only AuNRs are selectively visible in TEM images and D6-PAA is not visible due to the lower electronic contrast of the polymer, the assumption of the formation of a D6-PAA/AuNR nanohybrids is unambiguously confirmed by the results of absorption, PL, and Raman scattering given below. Thus, taking into account the above arguments and the fact of the significantly larger size of D6-PAA polymer macromolecule (the hydrodynamic diameter is 153 nm, Tab. 1), it is most likely that the studied 3-component 2I(4I)-HITC/D6-PAA/AuNR nanohybrids have the morphology schematically shown in Fig. 3.

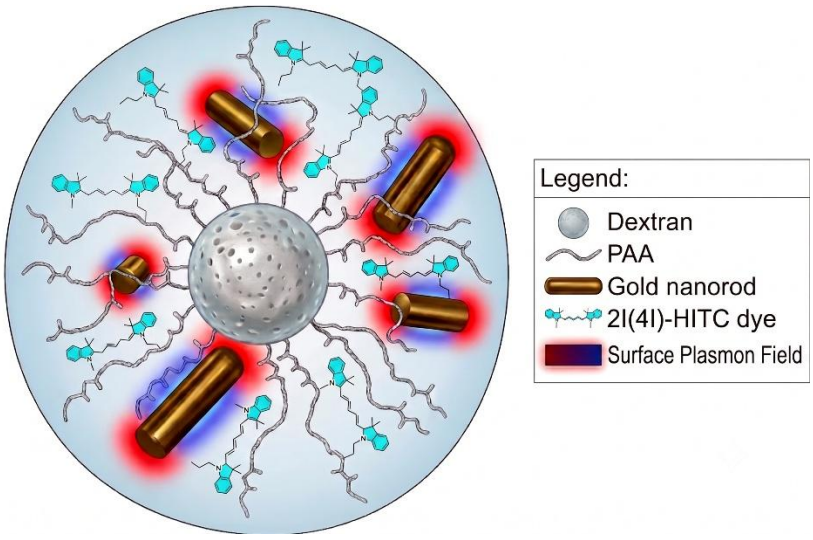


Fig. 3. Schematic presentation of 2I(4I)-HITC/D6-PAA/AuNR nanohybrid.

Free 2I-HITC and 4I-HITC dyes in water: absorption, photoluminescence and Raman scattering

Fig. 4 shows the normalized absorption (a) and PL (b) spectra of free 2I-HITC and 4I-HITC dyes in water, respectively. The absorption spectra of both dyes are similar in shape, each consisting of two distinct groups of absorption bands, Fig. 4(a). The first short-wavelength group contains two bands at 365 and 421 nm. The second long-wavelength group consists of three bands at 615, 681 and 751 nm. However, despite the spectral coincidence of the band maxima, there is a significant change of the relative intensities of the long-wavelength group bands. For PL, the PL spectra of molecules with different numbers of iodine atoms are characterized by different values of the PL Stokes shift relative to the absorption. Namely, the Stokes shift for 2I-HITC molecule is 16 nm larger compared to 4I-HITC, Fig. 4(b). Evidently, the differences of both absorption and PL spectra for 2I-HITC and 4I-HITC dyes is due to different perturbations of the quantum states of the dye molecule in molecules with different numbers of iodine atoms. In particular, 4I-HITC is more hydrophobic due to the presence of a larger number of iodine atoms, so the aggregate band is more pronounced in its spectrum.

Fig. 5 shows the concentration dependences of the absorption (optical density) (a) and PL intensity (b) of aqueous solutions of 2I-HITC and 4I-HITC. It can be seen that the absorption increases monotonically with increasing concentration, as expected. In turn, the concentration dependences of the PL intensity of both dyes are non-monotonic, having a maximum at 3×10^{-3}

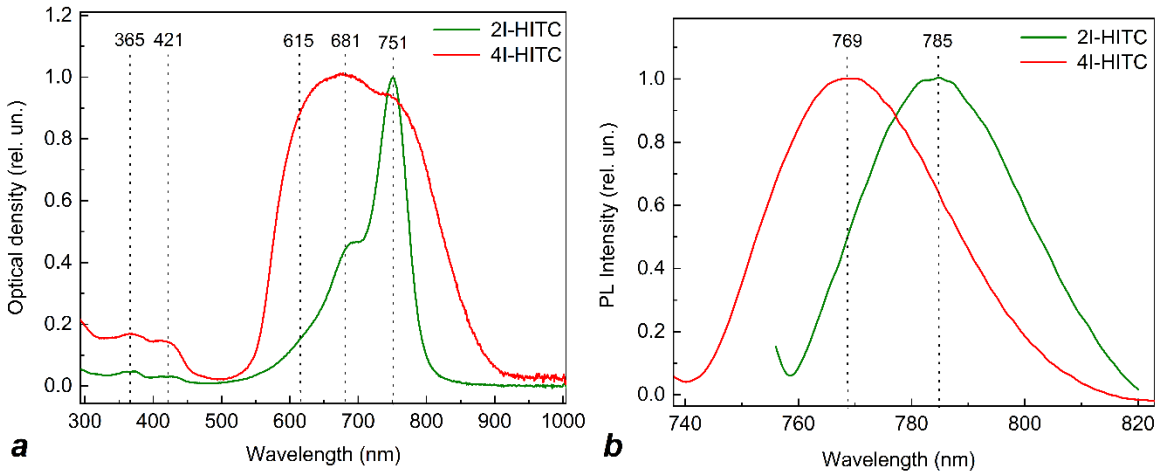


Fig. 4. Normalized absorption (a) and PL (b) spectra of free 2I-HITC and 4I-HITC dyes in water. Concentrations: 3×10^{-3} mg/mL (2I-HITC) and 4×10^{-3} mg/mL (4I-HITC). PL excitation: 750 nm (2I-HITC) and 730 nm (4I-HITC).

mg/mL for 2I-HITC and 4×10^{-3} mg/mL for 4I-HITC. Considering that the dyes under study are hydrophobic, when mixing their solution in DMSO with water, their aggregation should occur. Aggregation of photosensitizer dyes, as is known, leads to a decrease in their photodynamic efficiency. In turn, aggregation leads to PL quenching. Therefore, it is natural to assume that above values of concentrations at which PL quenching begins are optimal, since at higher concentrations intensive aggregation occurs, which is undesirable both for the use of the dyes as NIR fluorescent labels and as photosensitizers in PDT. Therefore, in further studies, when creating hybrid 2- and 3-component nanosystems, we used concentrations of 3×10^{-3} and 4×10^{-3} mg/mL for 2I-HITC and 4I-HITC respectively.

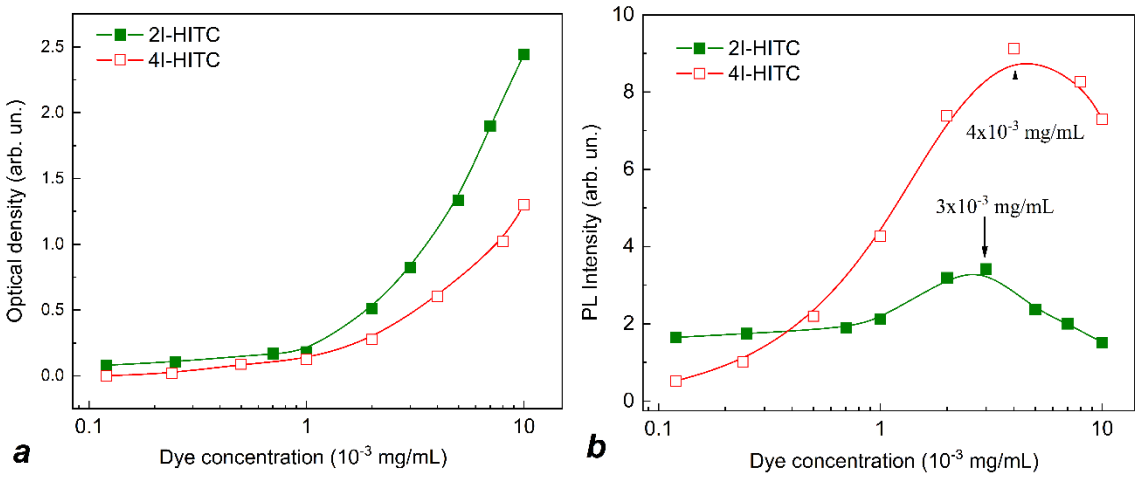


Fig. 5. Concentration dependences of absorption (optical density) (a) and PL intensity (b) of 2I-HITC and 4I-HITC aqueous solutions. Concentrations: 3×10^{-3} mg/mL (2I-HITC) and 4×10^{-3} mg/mL (4I-HITC). Optimal concentrations: 3×10^{-3} mg/mL (2I-HITC) and 4×10^{-3} mg/mL (4I-HITC).

The Raman spectra of 2I-HITC and 4I-HITC dyes (Fig. 6) were obtained from dried drops of aqueous solutions of the dyes deposited on an aluminum substrate under non-resonant 532 nm

(Fig. 6(a)) and resonant 785 nm (Fig. 6(b)) laser excitation. The spectra of 2I-HITC and 4I-HITC dyes at both excitation wavelengths contain groups of lines at close frequencies, but the ratio of line intensities for different dyes is significantly different. The spectra of both dyes contain the region of 122 – 1610 cm^{-1} with intense lines and the region at about 3000 cm^{-1} with very low intensity lines. In the following, we will consider only the intense region of the Raman spectrum in the 122 – 1610 cm^{-1} range.

The high-frequency region (822 – 1610 cm^{-1}) corresponds to vibrations of the unmodified HITC molecule, while the low-frequency group of lines (122 – 722 cm^{-1}), absent in the spectrum of the HITC molecule, corresponds to vibrations of the C–I bond. The high-frequency region contains the following groups of lines [50]: 1545–1610 cm^{-1} (stretching vibrations of the aromatic system of the indole heterocycle $\nu(C\ldots C)_{arom}$ in combination with the terminal group $C{=}N$); 1523–1540 cm^{-1} (asymmetric stretching vibration of the carbon chain); 1458–1463 cm^{-1} (deformation vibrations $\delta(CH_3)$ of geminal methyl groups at position 3,3' of the indolenine ring); 1362–1366 cm^{-1} (fully symmetrical stretching skeletal vibration of the entire heptamethine chain $\nu_{sym}(C\ldots C)_{chain}$); 1227–1300 cm^{-1} (synchronous plane $\delta(C-H)$ deformations of long chain and stretching vibrations $\nu(C-N)$ of nitrogen bonds embedded in the heterocycle); 1125–1187 cm^{-1} (plane deformations of indole rings and deformation vibrations of methyl groups $-CH_3$ in positions 1, 1', 3, 3'); 908–935 cm^{-1} (breath vibrations of the indolenine nucleus); 802–844 cm^{-1} (out-of-plane deformation vibrations $\gamma(C-H)$ of the polymethine chain (*trans*-configuration)). It is quite interesting and important that under non-resonant excitation at 532 nm, the high-frequency vibrational modes of the HITC molecule dominant in the Raman spectrum, while with resonant excitation at 785 nm, the lines corresponding to the vibrations of the C–I bond of iodine and carbon atoms dominate.

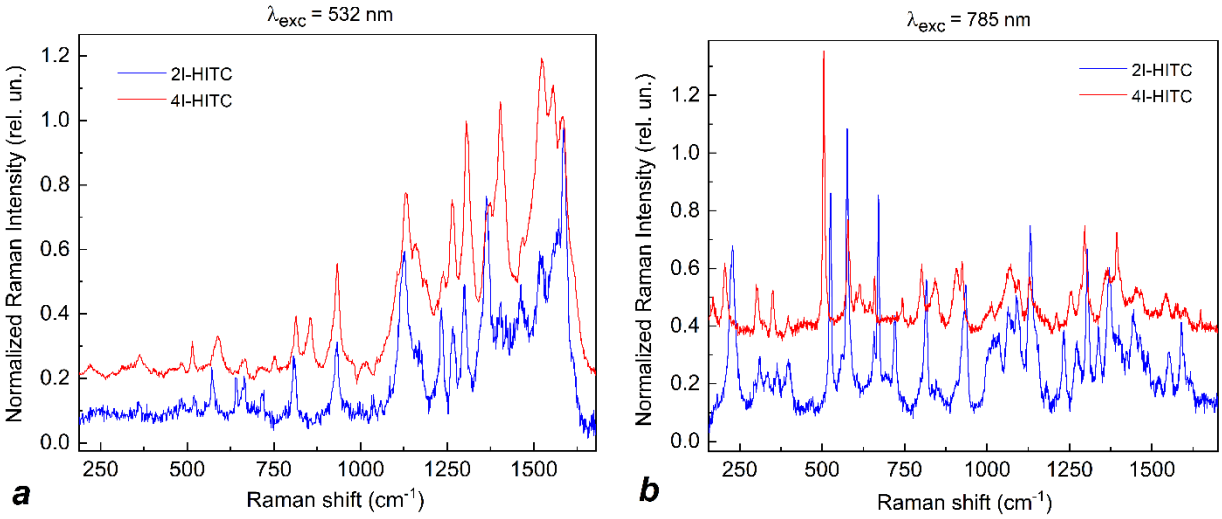


Fig. 6. Normalized Raman spectra of free 2I-HITC and 4I-HITC dyes in water under laser wavelength excitation of 532 nm (a) and 785 nm (b). Concentrations: 3×10^{-3} mg/mL (2I-HITC) and 4×10^{-3} mg/mL (4I-HITC). The spectra are shifted vertically for convenience.

D6-PAA/AuNRs in water: absorption

The absorption spectra of aqueous solutions of D6-PAA/AuNRs containing the AuNR660 and AuNR745 respectively are shown in Fig. 7. Absorption in the VIS range is due to the excitation of surface plasmon resonance (SPR) in AuNRs. The absorption spectrum of each sample contains two bands, i.e. short-wavelength T-bands at 518 and 513 nm (transverse SPR or T-SPR) and long-wavelength L-bands at 660 and 745 nm (longitudinal SPR or L-SPR) for gold nanorods with aspect ratios of 2.9 and 3.7, respectively. As expected, the L-band of nanorods with a higher aspect ratio is significantly shifted to the red by 85 nm. Accordingly, the aspect ratio of AuNR660 is 2.9, and one of AuNR745 is 3.7. The absorption band of the D6-PAA polymer has a maximum at 260 nm, which is outside the spectral range that we have studied.

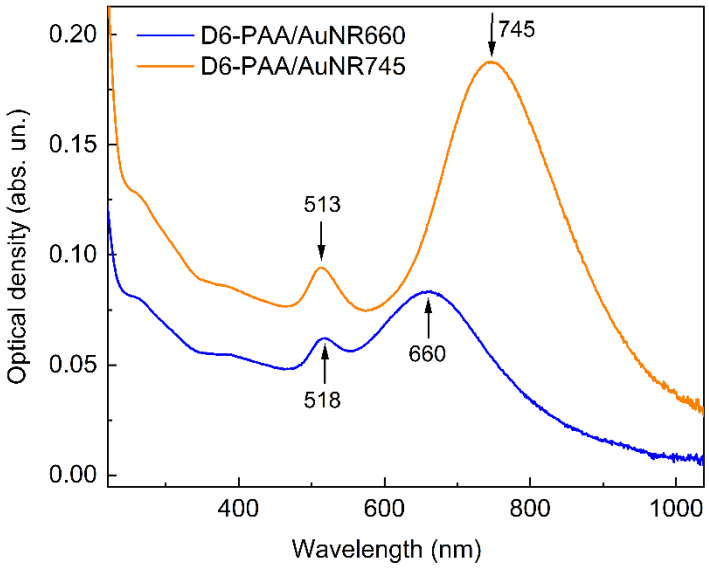


Fig. 7. Absorption spectra of D6-PAA/AuNR nanohybrids containing Au nanorods with aspect ratios of 2.9 (D6-PAA/AuNR660 sample) and 3.7 (D6-PAA/AuNR745 sample).

Multicomponent 2I-HITC(4I-HITC)/D6-PAA/AuNR nanohybrids in water: optical spectroscopy

Absorption

First, the binding of dye molecules to D6-PAA and D6-PAA/AuNR was checked. Next, the concentration effects in the optical spectra of the nanohybrids were investigated, namely the influence of polymer and gold concentration on the absorption and PL of dye molecules bound with nanohybrids. Studies of the effect of polymer and gold concentration for 2I(4I)-HITC/D6-PAA and 2I(4I)-HITC/D6-PAA/AuNRs nanohybrids were carried out at fixed optimal dye concentrations given above, namely: 3×10-3 mg/mL (2I-HITC) and 4×10-3 mg/mL (4I-HITC).

Fig. 8 shows the effect of polymer and gold concentration on the absorption spectra of nanohybrids. It can be seen (Fig. 8 (a,b)) that the absorption spectra of nanohybrids for both dyes change significantly both by spectral shape (there is a redistribution of the intensities of long- and short-wavelength peaks of the spectrum) and by total intensity. This proves the fact of binding of 2I-HITC and 4I-HITC molecules both to bare D6-PAA polymer and to nanohybrids containing Au NRs of both types. The change in the spectral shape and total intensity of the spectra upon binding dye molecules to nanohybrids containing Au NRs is particularly strong. Given the

resonance of the dye absorption spectrum with the longitudinal plasmonic L-mode of the nanorods (660 and 745 nm depending on the type of NRs), this is due to two reasons. The first is trivial and is associated with the addition of the absorption spectrum of gold nanorods to the total spectrum. However, the main reason for the observed changes in the absorption spectrum is plasmonic effects – both the overall enhancement of the dye light absorption and the redistribution of the intensities of individual peaks due to strong frequency dependence of the plasmonic enhancement factor (EF).

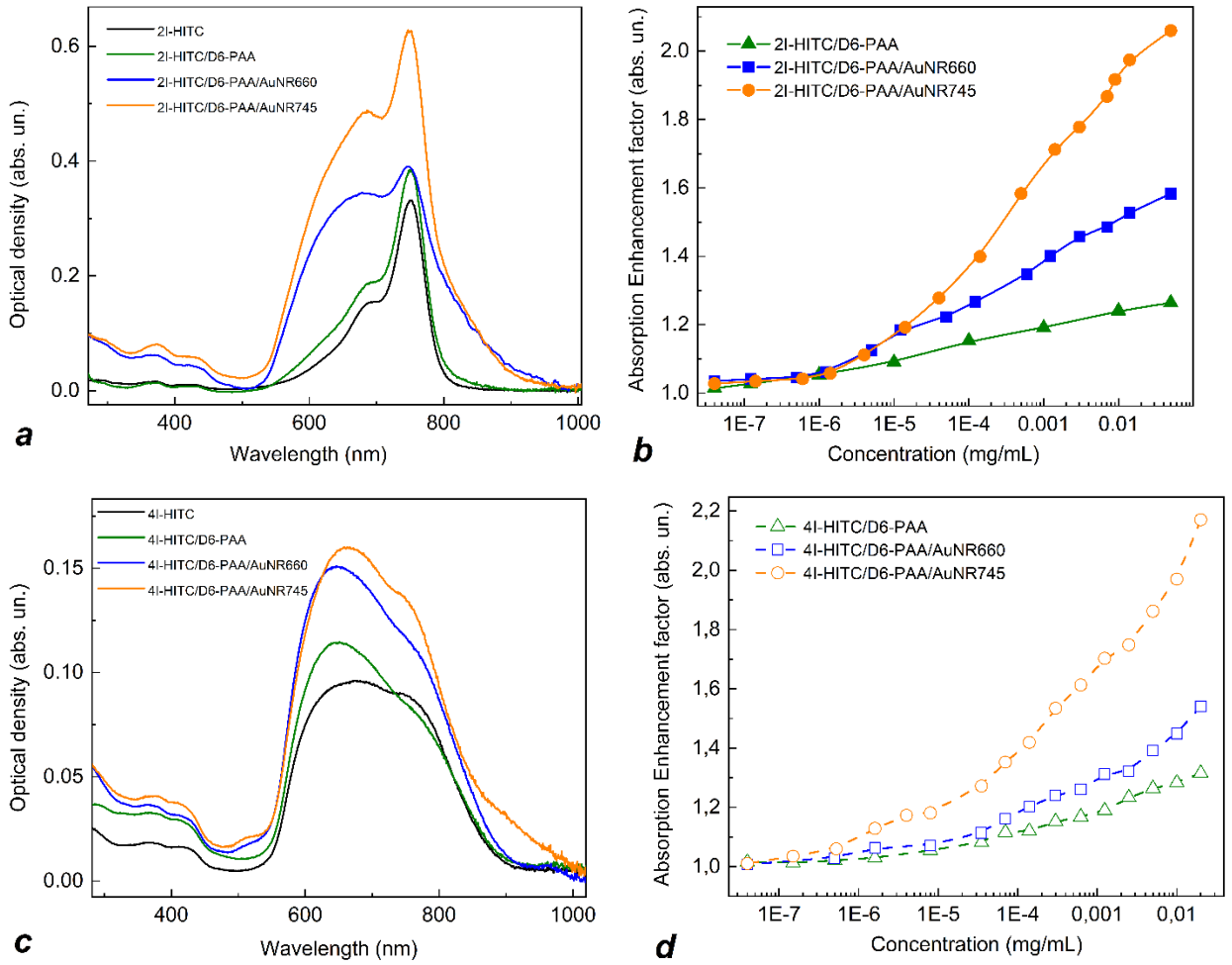


Fig. 8. Absorption of free 2I(4I)-HITC and nanohybrids of 2I(4I)-HITC/D6-PAA and 2I(4I)-HITC/D6-PAA/AuNRs in water: (a,b) – absorption spectra of the systems containing 2I-HITC (a) and 4I-HITC (c) respectively; (c,d) – dependence of the absorption EF on the concentration of D6-PAA (for systems without AuNRs) or gold (for systems containing AuNRs). The EFs are given relative to free 2I(4I)-HITC in water. The dye concentrations are constant and equal to the optimal values given above (3×10^{-3} mg/mL for 2I-HITC and 4×10^{-3} mg/mL for 4I-HITC). The spectra shown on panels (a) and (c) correspond to samples with maximum PL intensity (see Figs. 9(b,d)).

Since, as noted above, the absorption spectrum of the 2I(4I)-HITC/D6-PAA and 2I(4I)-HITC/D6-PAA/AuNRs nanohybrid is not the usual sum of the spectra of the individual components, to clarify the influence of the polymer and AuNRs on the dye absorption, we subtracted the absorption spectrum of AuNR from the spectrum of the 2I(4I)-HITC/D6-PAA/AuNR nanohybrid. Because the polymer absorbs only in the UV region, its contribution to the absorption spectra was not subtracted. Next, the total optical density of the absorption spectrum

of the dye in the hybrid was divided by the corresponding value for the free dye. In this way, we determined the EF of light absorption by the dye due to its inclusion in the nanohybrid. The results are shown on Fig. 8(b) for nanohybrids containing the 2I-HITC dye and on Fig. 8(d) for those containing 4I-HITC. It can be seen that in the studied concentration range, increasing the concentration of both polymer and gold leads to a monotonic increase in the absorption EF for both dyes.

As can be seen from Fig. 8(b,d), enhanced dye absorption is occurred not only in 2I(4I)-HITC/D6-PAA/AuNRs nanohybrids containing plasmonic AuNRs and polymer, but also in 2I(4I)-HITC/D6-PAA systems without NRs. Such an effect was reported in our recent works for nanohybrids containing Dextran grafted-PAA polymer and photosensitizers ZnTPP [47,48] and temoporfin [44]. It is associated with the fact that the D6-PAA polymer prevents the aggregation of dye molecules, which leads to an increase in dye absorption. However, the increase in absorption due to the polymer is not significant. A sufficiently higher absorption enhancement is observed for both dyes bound to nanohybrids containing plasmonic AuNRs. Increasing the gold concentration leads to a decrease in the mean distance between the dye molecules and AuNRs in nanohybrid, which in turn leads to an increase in the plasmonic absorption enhancement, as confirmed by experimental data. Such plasmonic absorption enhancement is noticeably higher for the 2I(4I)-HITC/D6-PAA/AuNR745 systems containing NRs with a higher aspect ratio. This result is due to the fact that, as is well known in plasmonics [51,52], more intense plasmonic hot spots appear near the ends of nanorods with a higher aspect ratio, where the main enhancement of optical processes in molecules located in the plasmonic field occurs.

Photoluminescence

The effect of the polymer and gold concentration on the PL of the dyes is illustrated in Fig. 9. It can be seen that, similarly to the absorption, the binding of both 2I-HITC and 4I-HITC dyes to the D6-PAA polymer leads to a slight increase in the PL intensity. As noted above, this is due to the fact that the polymer reduces the aggregation of hydrophobic dye molecules, which slightly increases the PL quantum yield compared to an aqueous solution of free dye molecules. This effect is similar to that observed in our recent works [44,47,48] for other photosensitizers bound with dextran grafted-PAA polymer.

Meanwhile, the concentration of gold NRs has a much stronger effect on the PL intensity of the dyes. Fig. 9(b,d) shows the dependence of the PL EF of the dyes on the AuNRs concentration. The PL EF was determined as the ratio of the total PL intensity of the dye in the 2I(4I)-HITC/D6-PAA or 2I(4I)-HITC/D6-PAA/AuNRs nanohybrid to the intensity of the free dye in water. It can be seen that the dependences of the EF (PL intensity) on the AuNRs concentration are non-monotonic. Initially, an increase in the AuNRs leads to an increase in the PL intensity, a maximum is reached, and then PL quenching occurs. Such trend is observed for both 2I-HITC and 4I-HITC dyes and both AuNR660 and AuNR745 gold NRs. The gold concentrations at which maximum PL enhancement is achieved were determined as follows: 1.9×10^{-5} mg/mL for 2I-HITC/D6-PAA/AuNR660, 1.8×10^{-4} mg/mL for 2I-HITC/D6-PAA/AuNR745, 5.0×10^{-5} mg/mL for 4I-HITC/D6-PAA/AuNR660, and 8.0×10^{-6} mg/mL for 4I-HITC/D6-PAA/AuNR745.

Since the dye molecules are bound to the D6-PAA/AuNRs hybrids, they are located in a plasmonic field, and therefore the PL enhancement is obviously of plasmonic nature. However, in

addition to plasmonic enhancement, another competing mechanism for the concentration dependence of the PL intensity is the non-radiative resonant energy transfer from the excited donor to the acceptor, which leads to the quenching of the PL with a decrease in the distance in the donor-acceptor pair. The most common mechanism of non-radiative resonant energy transfer is the dipole-dipole Förster mechanism – FRET. As is known [53–55], in pair of a dye molecule-gold NP with a resonant overlap of the PL spectrum of the molecule and the surface plasmon resonance of the Au NP, the donor is usually the dye molecule, and the acceptor is the Au NP. Since the plasmon electric field strength depends on the distance to the metal NP as $E_{sp} \propto r^{-3}$ [53,54], and the FRET rate as $\gamma_{FRET} \propto r^{-6}$ [55], it is clear that the increase in the PL intensity at lower concentrations is due to plasmon enhancement, and the quenching at high concentrations is due to the FRET phenomenon.

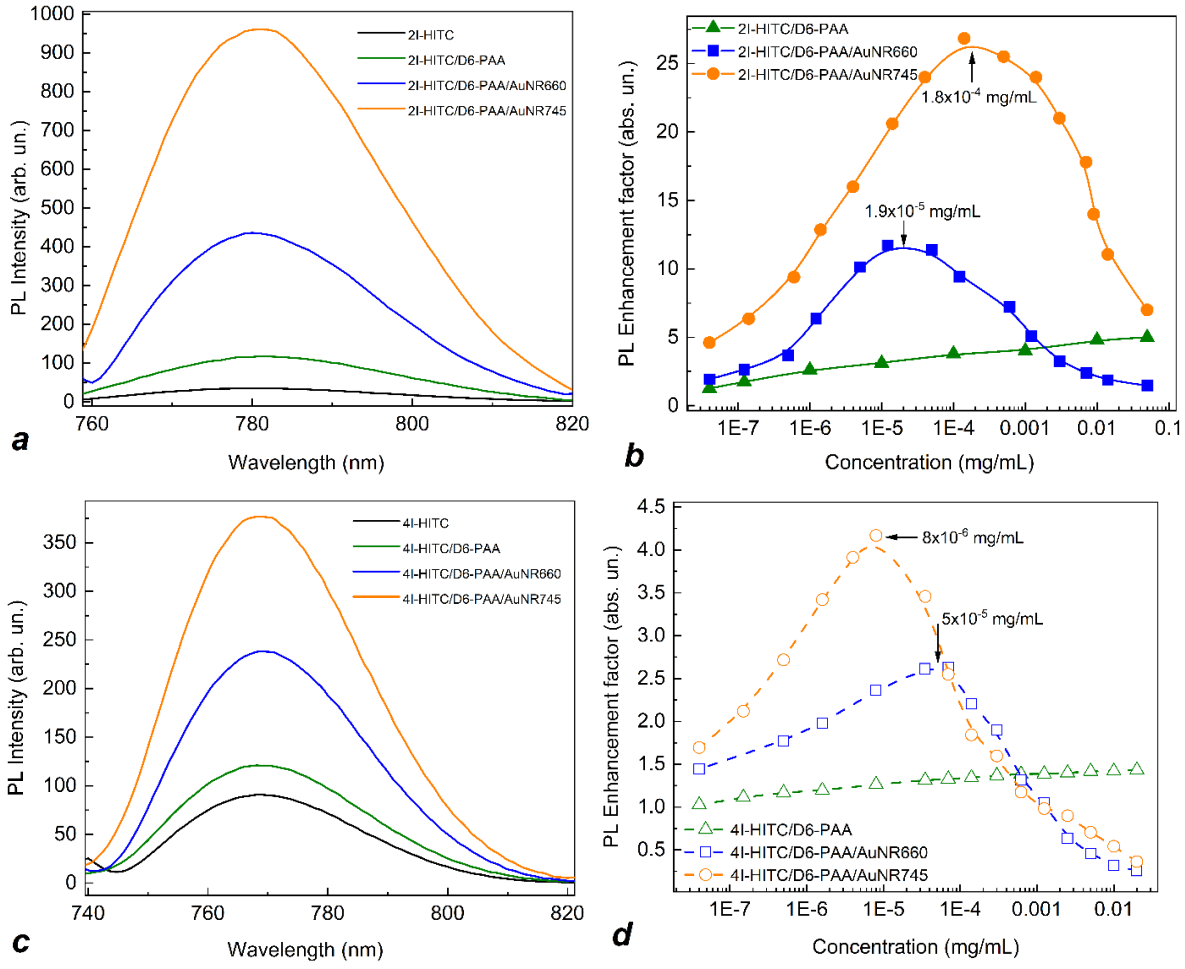


Fig. 9. PL of free 2I(4I)-HITC and nanohybrids of 2I(4I)-HITC/D6-PAA and 2I(4I)-HITC/D6-PAA/AuNRs in water: PL spectra of the systems containing 2I-HITC (a) and 4I-HITC (c) respectively; dependences of the PL EF on the concentration of D6-PAA (for systems without AuNRs) or gold (for systems containing AuNRs) for the systems containing 2I-HITC (b) and 4I-HITC (d) respectively. The EFs are given relative to free 2I(4I)-HITC in water. The dye concentrations are constant and equal to the optimal values given above (3×10^{-3} mg/mL for 2I-HITC and 4×10^{-3} mg/mL for 4I-HITC). The spectra presented on panels (a) and (c) correspond to the samples with the optimal values of concentration of dyes, polymer and gold NRs given above.

Figs. 8(b,d) show that, similarly to the absorption, a higher PL enhancement is provided by Au NRs with a larger aspect ratio, i.e. AuNR745. There are two reasons for this. The first is a higher strength of the plasmon field in hot spots near the ends of the NR for AuNR745 than for AuNR660. The second is a higher overlap of the PL spectrum of the dyes (for 2I-HITC the maximum PL is at 780 nm, for 4I-HITC at 768 nm) with the plasmon L-mode of AuNR745 (745 nm) than with the L-mode of AuNR660 (660 nm).

Another interesting fact is that the concentrations at which the maximum PL intensity is observed for nanohybrids containing the 4I-HITC dye (4I-HITC/D6-PAA/AuNR660(745)) are approximately an order of magnitude lower than for nanohybrids with the 2I-HITC dye (2I-HITC/D6-PAA/AuNR660(745)), Fig. 9(b,d). This means that the FRET quenching of PL in nanohybrids with 4I-HITC begins at lower concentrations (larger mean distance between AuNRs and dye molecules) than with 2I-HITC. Accordingly, in nanohybrids in which PL quenching begins at higher concentrations (smaller molecule-NR distances), a higher plasmon PL enhancement should be achieved, in agreement with the experimental results. Indeed, the maximum PL EFs for the nanohybrids 2I-HITC/D6-PAA/AuNR745 (26.8 times) and 2I-HITC/D6-PAA/AuNR660 (11.7 times) are significantly higher than those for 4I-HITC/D6-PAA/AuNR745 (4.2 times) and 2I-HITC/D6-PAA/AuNR660 (2.6 times). Thus, it can be concluded that the efficiency of non-radiative energy transfer from 4I-HITC molecules to AuNRs is noticeably higher than that from 2I-HITC. Accordingly, this provides a higher plasmon enhancement for nanohybrids with 2I-HITC than for 4I-HITC. In turn, higher plasmon enhancement is achieved with the larger aspect ratio AuNRs, namely AuNR745. As a result, 2I-HITC/D6-PAA/AuNR745 nanohybrids exhibit the highest potential for practical applications, in particular as fluorescent labels for diagnostics and in photodynamic therapy.

Raman scattering (SERS)

Similar to the free 2I(4I)-HITC molecules, the Raman spectra of the nanohybrids 2I(4I)-HITC/D6-PAA and 2I(4I)-HITC/D6-PAA/AuNR660(745) were studied at two laser excitation wavelengths – 532 nm (Fig. 10(a,c)) and 785 nm – Fig. 10(b,d)). Similar to Raman spectra of free dyes, the spectra of nanohybrids contain the region of 122 – 1610 cm^{-1} with intense lines and the region at about 3000 cm^{-1} of very low intensity lines. The region around 3000 cm^{-1} also contains weak Raman bands arising from the polymer. Similar to the spectra of free dyes, the region of nanohybrid spectra near 3000 cm^{-1} due to its very low intensity will not be considered further. Compared with the Raman spectra of free dyes, the spectra of dyes in the nanohybrids are characterized by a redistribution of the intensities of many lines, and a spectral shift is observed for some lines. This, together with the absorption and PL data, proves the fact of binding of 2I-HITC and 4I-HITC molecules to hybrid macromolecules.

However, the main effect observed in the spectra of dyes due to their inclusion in the composition of nanohybrids is a significant enhancement of the Raman intensity, which is observed both at 532 nm and 785 nm excitation, Fig. 10. It can be seen that at 785 nm excitation the enhancement is an order of magnitude higher than at 532 nm excitation. As can be seen from Fig. 7, both laser excitation at 532 nm and at 785 nm are close to the resonance with the plasmon transverse T-mode (518 nm for AuNR660, 513 nm for AuNR745) and longitudinal L-mode (660 nm for AuNR660, 745 nm for AuNR745), respectively. Thus, the enhancement of the Raman

intensity has the plasmonic nature, i.e., it is a manifestation of the SERS phenomenon. The fact of observing intense SERS indicates the close spatial arrangement of 2I(4I)-HITC molecules and AuNRs, which again proves the fact of the presence of dye molecules in the composition of nanohybrids.

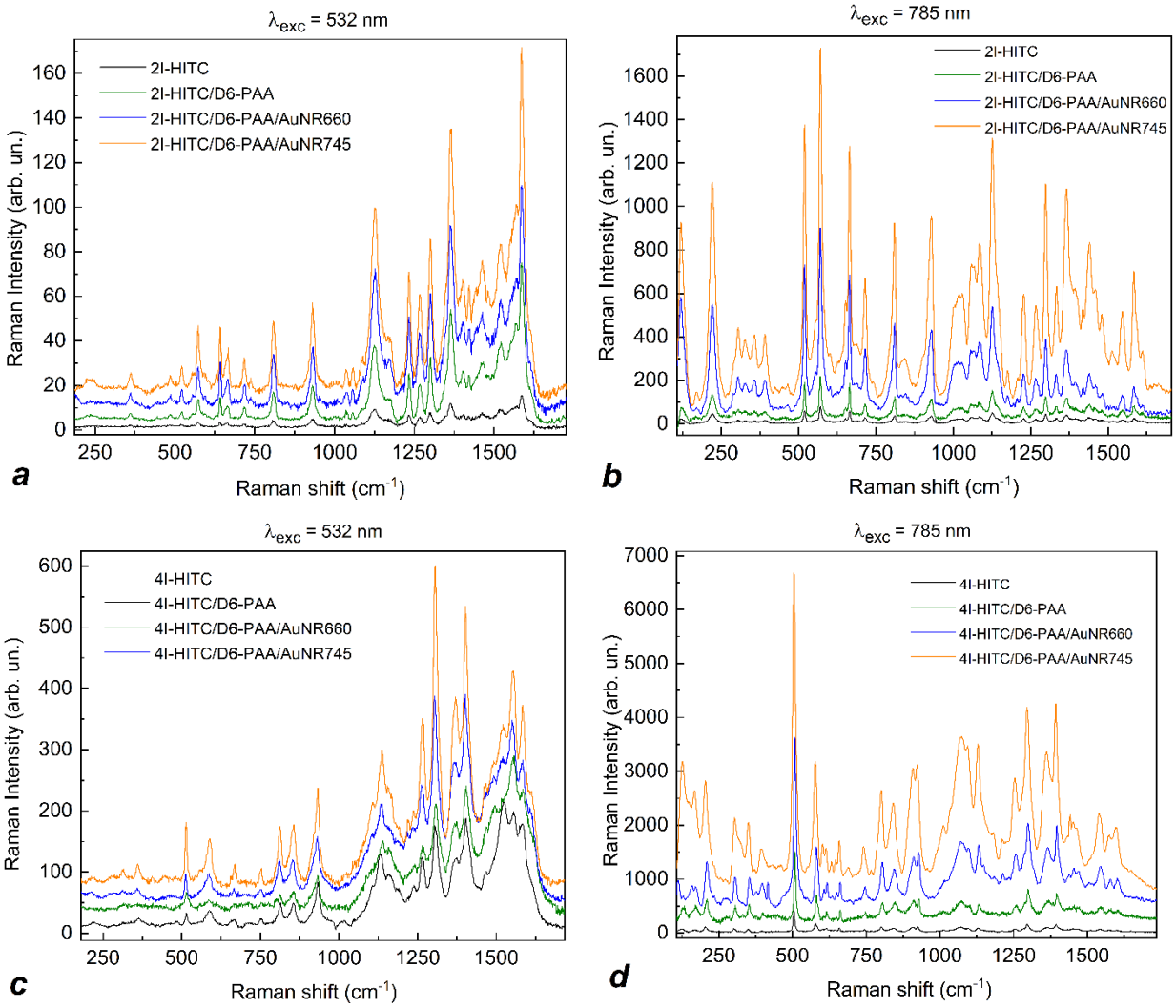


Fig. 10. Raman spectra of free 2I(4I)-HITC and nanohybrids of 2I(4I)-HITC/D6-PAA and 2I(4I)-HITC/D6-PAA/AuNRs in water under different laser excitation wavelengths of 532 nm and 785 nm: (a) – spectra of the systems containing 2I-HITC under excitation of 532 nm; (b) – 2I-HITC, 785 nm; (c) – 4I-HITC, 532 nm; (d) – 4I-HITC, 785 nm. Concentrations of the components: 3×10^{-3} mg/mL (2I-HITC), 4×10^{-3} mg/mL (4I-HITC); 1.8×10^{-4} mg/mL (Au).

It is clear that since the intensity of the plasmon L-resonance is much higher than one of the T-resonance, the SERS enhancement under 785 nm excitation should be noticeably higher than under 532 nm excitation. This conclusion is convincingly confirmed experimentally, since the intensity of the SERS lines under 785 nm excitation is an order of magnitude greater than under 532 nm excitation, Fig. 10. It is also seen that similarly to the PL, AuNR745 provide significantly higher SERS enhancement than AuNR660. This is due to the significantly lower detuning of the 785 nm excitation wavelength relative to the plasmonic L-mode in AuNR745 (40 nm) than in AuNR660 (125 nm).

The experimental values of the SERS EF, denoted further as $F_{SERS,\Sigma}$, were determined as the ratio of the total intensity of the Raman spectrum of the 2I(4I)-HITC/D6-PAA or 2I(4I)-HITC/D6-PAA/AuNR660(745) nanohybrid to the total intensity of the spectrum of free dye molecules. The obtained values of $F_{SERS,\Sigma}$ are given in Table 2. It should be noted that the given values of the SERS EF were determined at the concentrations of the nanohybrid components (dyes, polymer, gold) at which the maximum PL intensity of the corresponding nanohybrid was observed. It is noteworthy that, similarly to the PL EFs, the SERS EFs for nanohybrid with the 2I-HITC dye are higher than for nanohybrid with 4I-HITC. This is understandable because, as mentioned above, due to the more intense FRET, the maximum PL intensity for 4I-HITC/D6-PAA/AuNRs is achieved at a lower gold concentration (and therefore a higher mean dye-NR distance) than for 2I-HITC/D6-PAA. Correspondingly, the smaller distance leads to lower plasmonic enhancement. This is further discussed below, where the experimental and calculated values of the SERS EFs are compared.

Table 2. Comparison of experimental and calculated SERS EFs ($F_{SERS,\Sigma}$) for 2I-HITC and 4I-HITC dyes in plasmonic field of AuNR660 and AuNR745. Experimental values correspond to samples with dye, polymer and gold concentrations providing maximum PL intensity.

Sample		2I-HITC/D6-PAA/AuNR660	2I-HITC/D6-PAA/AuNR745	4I-HITC/D6-PAA/AuNR660	4I-HITC/D6-PAA/AuNR745
$F_{SERS,\Sigma}$, 532 nm	Exper.	3.3	3.1	3.2	3.1
	Calc.	4.1	3.7	4.2	3.9
$F_{SERS,\Sigma}$, 785 nm	Exper.	7.2	25.4	5.1	15.6
	Calc.	12.0	39.2	12.2	40.1

Calculation of SERS enhancement factors

To substantiate the qualitative explanation of the SERS enhancement of dye molecules in nanohybrids, we calculated the plasmonic SERS EFs for dye molecules hybridized with AuNRs. The calculations were performed within the framework of the analytical model of plasmonic enhancement by Boyd et al. [56]. The plasmonic enhancement of the electric field amplitude at the frequency ω is taken into account by introducing the amplitude EF or the so-called local field correction factor. For a molecule located directly near the surface of a metal nanoparticle, Boyd's theory gives the following expression for the local field correction factor:

$$L(\omega) = \left| \frac{E_{loc}(\omega)}{E_0(\omega)} \right|, \quad (1)$$

where $E_0(\omega)$ and $E_{loc}(\omega)$ are the amplitudes of the exciting (laser) wave field and the plasmon enhanced local field near the NP surface, respectively. According to Boyd's theory [56], the local field correction factor is expressed as

$$L(\omega)=\left|\frac{\frac{\varepsilon(\omega)}{\varepsilon_m}D^{-1}}{\frac{\varepsilon(\omega)}{\varepsilon_m}-1+D^{-1}\left[1+i\frac{4\pi^2V\left(1-\varepsilon(\omega)\right)}{3\lambda^3}\varepsilon_m^{1/2}\right]}\right|, \tag{2}$$

where $\varepsilon(\omega)$ and ε_m are the dielectric constants of a metal NP and environment respectively, D is the geometric factor depending on the NP shape, V is the NP volume, and λ is the wavelength. Since, NR has two non-equivalent axes, it has two different geometric factors (longitudinal and transversal), which are expressed as

$$D_L=\frac{1-e^2}{e^2}\left(\frac{1}{2e}\ln\frac{1+e}{1-e}-1\right) \quad \text{and} \quad D_T=\frac{1}{2}(1-D_L)\ , \tag{3}$$

where $e=\sqrt{1-1/R^2}$ is the eccentricity, and R is the aspect ratio of NR.

The NRs are located in the volume of the nanohybrid arbitrarily, and therefore they oriented arbitrarily relative to the vector $\boldsymbol{E}$ of the exciting laser wave. Therefore, the contribution to the effective local field correction factor will be given by both of its plasmon modes. In addition, the dye molecules are located arbitrarily relative to different parts of the NR, and therefore they will be in some averaged effective plasmon field, the local correction factor of which can be expressed as:

$$L_{NR}(\omega)=\sqrt{\frac{L_L^2+L_T^2}{2}}\ . \tag{4}$$

Since the plasmon fields enhances the fields of both exciting laser photon and scattered photon, the enhanced SERS intensity at the frequency ω_s is expressed as

$$I_{SERS}(\omega_s)=F_{SERS}(\omega_l,\omega_s)I_{s0}(\omega_s)\ , \tag{5}$$

where

$$F_{SERS}(\omega_l,\omega_s)=L^2(\omega_l)L^2(\omega_s) \tag{6}$$

is the SERS EF at the frequency ω_s. Here, $I_{s0}(\omega_s)$ is the Raman intensity of the free molecule at the frequency ω_s, and ω_l, ω_s are the laser and scattered photon frequency, respectively. Similar to experimental SERS EF presented in Tab. 2, we calculated the total SERS EF as the ratio of the total intensity of SERS spectrum calculated by Exp. (5) and the total intensity of Raman spectrum of the free dye molecules:

$$F_{SERS,\Sigma}=\frac{\int_{\omega_{s,\min}}^{\omega_{s,\max}}I_{SERS}(\omega_s)d\omega_s}{\int_{\omega_{s,\min}}^{\omega_{s,\max}}I_{s0}(\omega_s)d\omega_s}\ . \tag{7}$$

The optical constants for Au were taken from Ref. [57], the dielectric constant of environment were taken to be $\varepsilon_m = 1.33^2$, the length, diameter and aspect ratio of NRs were taken from TEM data.

The calculated total SERS EFs $F_{SERS,\Sigma}$ of the 2I-HITC and 4I-HITC dyes located directly near the surface of the AuNR660 and AuNR745 nanorods are shown in Table 2. As expected, the

calculated $F_{SERS,\Sigma}$ values for both dyes are significantly higher for excitation by a 785 nm laser than for 532 nm. Also, the calculated $F_{SERS,\Sigma}$ for AuNR745 are higher compared to AuNR660. The same effects are observed experimentally. The physical reasons for these two effects are discussed above.

It can be seen that the calculated $F_{SERS,\Sigma}$ for both dyes for the same AuNR under the same excitation are the same, Tab. 2. The experimental $F_{SERS,\Sigma}$ under the same conditions for different dyes differ, namely $F_{SERS,\Sigma}$ for 4I-HITC is lower than for 2I-HITC. It is also evident that the experimental $F_{SERS,\Sigma}$ for both dyes combined with either type of AuNRs at both excitation wavelengths are lower than the corresponding calculated values. The reason for these two facts is that in real systems the dye molecules are at a certain distance from the NRs, while in the theoretical model the molecules are considered to be on the surface of the NRs. Since the amplitude of the plasmon field decreases with distance from NR surface as $1/r^3$, it is obvious that the calculated $F_{SERS,\Sigma}$ for molecule on the surface of the NR is the maximum achievable. That is a reason why the experimental $F_{SERS,\Sigma}$ are lower than the calculated ones. Therefore, the larger underestimation of the $F_{SERS,\Sigma}$ experimental values for the 4I-HITC/D6-PAA/AuNR nanohybrid compared to those calculated for 2I-HITC/D6-PAA/AuNR indicates that in nanohybrids with 4I-HITC the mean distance between the dye molecules and AuNRs is larger (respectively, the concentration of AuNRs nanorods is lower) than in nanohybrids with 2I-HITC. This conclusion is fully consistent with the PL data presented above.

Conclusions

In this work, we developed and investigated water-soluble 3-component nanohybrid complexes comprising iodinated heptamethinecyanine NIR dyes (2I-HITC or 4I-HITC), star-like dextran-graft-polyacrylamide copolymer (D6-PAA), and gold nanorods (AuNRs) as potential platform for biomedical NIR imaging and sensing applications. The synthesized D6-PAA copolymer provided a stable macromolecular matrix that efficiently encapsulated AuNRs and reduced hydrophobic dye aggregation. By matching the longitudinal plasmon resonance of the AuNRs at 660 nm (AuNR660) and 745 nm (AuNR745) with the NIR absorption and emission bands of the dyes within the biological transparency window, significant plasmonic enhancement of both photoluminescence (SEPL) and Raman scattering (SERS) was achieved.

The plasmonic optical response exhibited a strong dependence on component concentrations and AuNR aspect ratios. The nanohybrids containing AuNRs with a higher aspect ratio (AuNR745) provided superior enhancement due to stronger local electromagnetic field in hot spots at the nanorod tips and greater spectral overlap with the dyes spectra. Crucially, the 2I-HITC/D6-PAA/AuNR745 nanohybrid demonstrated the highest PL enhancement factor (up to 26.8-fold) and SERS enhancement factor (up to 25.4-fold under 785 nm laser excitation). Compared to 4I-HITC, the 2I-HITC dye suffered less from non-radiative Förster resonance energy transfer (FRET) quenching, enabling higher plasmonic enhancement. Analytical calculations of local field correction factors based on Boyd's theory closely confirmed the experimental SERS

trends, further validating the spatial proximity of the functional components within the polymer matrix.

Overall, the observed significant plasmonic enhancement of light absorption, photoluminescence, and Raman scattering in aqueous colloidal solutions of the three-component 2I-HITC/D6-PAA/AuNR745 nanohybrid suggests its potential for applications in NIR optical bioimaging and diagnostic SERS sensing. It should be noted, however, that this conclusion is based on physicochemical studies. Further specialized biological studies are required to evaluate the diagnostic and therapeutic (photodynamic) efficacy of the investigated nanohybrids in actual living systems.

Author information

Corresponding Author

Oleg Yeshchenko – Faculty of Physics, Taras Shevchenko National University of Kyiv, Kyiv, Ukraine; ORCID: orcid.org/0000-0001-8927-5673, E-mail: oleg.yeshchenko@knu.ua

Authors

Oles Fedotov – Faculty of Physics, Taras Shevchenko National University of Kyiv, Kyiv, Ukraine; ORCID: orcid.org/0009-0003-9401-9078, E-mail: oles.fedotov@gmail.com

Pavlo Khort – Faculty of Physics, Taras Shevchenko National University of Kyiv, Kyiv, Ukraine; ORCID: orcid.org/0000-0002-1169-2431, E-mail: pavlo.khort@knu.ua

Dmytro Kobzev – Institute of Functional Materials Chemistry, SSI "Institute for Single Crystals" of NAS of Ukraine, Kharkiv, Ukraine; ORCID: orcid.org/0000-0002-7731-6420; E-mail: kobzevua@yahoo.com

Anatoliy Tatarets – Institute of Functional Materials Chemistry, SSI "Institute for Single Crystals" of NAS of Ukraine, Kharkiv, Ukraine; ORCID: orcid.org/0000-0003-4406-7883; E-mail: tatarets@isc.kh.ua

Mykola Ischenko – Faculty of Chemistry, Taras Shevchenko National University of Kyiv, Kyiv, Ukraine; ORCID: orcid.org/0000-0002-0851-1679, E-mail: ischenko_mv@knu.ua

Volodymyr Doroschuk – Faculty of Chemistry, Taras Shevchenko National University of Kyiv, Kyiv, Ukraine; ORCID: orcid.org/0000-0001-6703-1926, E-mail: doroschuk@univ.kiev.ua

Pavlo Virych – Faculty of Chemistry, Taras Shevchenko National University of Kyiv, Kyiv, Ukraine; ORCID: orcid.org/0000-0002-1463-1992, E-mail: pavlo.virych@knu.ua

Natalia Kutsevol – Faculty of Chemistry, Taras Shevchenko National University of Kyiv, Kyiv, Ukraine; ORCID: orcid.org/0000-0002-1468-4111, E-mail: nataliya.kutsevol@knu.ua

Author Contributions

O. Y. conceptualization, methodology, project administration, formal analysis, funding acquisition, calculation, investigation, writing – original draft, writing – review & editing;

O. F. data curation, formal analysis, investigation; P. K. data curation, formal analysis, investigation; D. K. data curation, investigation; A. T. data curation, investigation; M. I. data curation, investigation;
V. D. data curation, investigation; P. V. conceptualization, funding acquisition, data curation, formal analysis, investigation; N. K. conceptualization, formal analysis, investigation.

Data availability

All data supporting the findings of this study are available within the article.

Declarations

Competing Interests. The authors declare no competing interests.

Funding

This work was supported by National Research Foundation of Ukraine through the project 2025.07/0024 “Physical principles of influence on electronic processes in metalorganic nanohybrids as innovative materials for photonics and medicine”.

References

1. Jain PK, El-Sayed IH, El-Sayed MA (2007) Au nanoparticles target cancer. *Nano Today* **2**:18–29
2. Shanmugam V, Selvakumar S, Yeh CS (2014) Near-infrared light-responsive nanomaterials for cancer phototherapy. *Chem Soc Rev* **43**:6254–6287
3. Khoramipour M, Chegeni MM, Moradbeygi F, Najafi F, Kabarkouhi Z, Poodeh SH, Larijani SF, Ghaemi A, Jevinani HN, Goodarzi A, Beram FM, Moeinzadeh A, Moghaddam NA, Farmani AR, Bernkop-Schnürch A (2026) Gold nanoparticles as a versatile theranostic platform in oncology: A comprehensive point of view on synthesis, properties, functionalization, and clinical translation. *Colloid Interface Sci Commun* **72**:100880
4. Wang J, Gao X, Feng L, Zhang D, Lv S, Li X, Liu Q, Yu D, Xing M, Li D, Suo L, Moua H, Song J (2025) Advances in near-infrared responsive functional nanocomposites for bioimaging and antitumor research. *J Control Release* **384**:113904
5. Yang Y, Xie Y, Zhang F (2023) Second near-infrared window fluorescence nanoprobes for deep-tissue in vivo multiplexed bioimaging. *Adv Drug Deliv Rev* **193**:14697
6. Wu H, Li X, Liu Z, Song F, Cai R, Chen H, Zhang G (2026) Advances in near-infrared fluorescence imaging for biomedicine. *Coord Chem Rev* **561**:217892
7. Smith AM, Mancini MC, Nie S (2009) Bioimaging: second window for in vivo imaging. *Nat Nanotechnol* **4**:710–711
8. Weissleder R (2001) A clearer vision for in vivo imaging. *Nat Biotechnol* **19**:316–317
9. Mishra A, Behera RK, Behera PK, Mishra BK, Behera GB (2000) Cyanines during the 1990s: A review. *Chem Rev* **100**:1973–2012
10. Lorenz AS, Buabeng ER, Taratula O, Taratula O, Henary M (2021) Near-Infrared Heptamethine Cyanine Dyes for Nanoparticle-Based Photoacoustic Imaging and Photothermal Therapy. *J Med Chem* **64**:8798–8805

11. Schaafsma BE, Mieog JSD, Hutteman M, van der Vorst JR, Kuppen PJK, Löwik CWGM, Frangioni JV, van de Velde CJH, Vahrmeijer AL (2011) The clinical use of indocyanine green as a near-infrared fluorescent contrast agent for image-guided oncologic surgery. *J Surg Oncol* **104**:323–332
12. Egloff-Juras C, Bezdetnaya L, Dolivet G, Lassalle HP (2019) NIR fluorescence-guided tumor surgery: new strategies for the use of indocyanine green. *Int J Nanomedicine* **14**:7823–7838
13. Qiu Y, Yuan B, Cao Y, He X, Akakuru OUA, Lu L, Chen N, Xu MX, Wu A, Li J (2023) Recent progress on near-infrared fluorescence heptamethine cyanine dye-based molecules and nanoparticles for tumor imaging and treatment. *WIREs Nanomed Nanobiotechnol* **15**:e1910
14. Chen X, Lin Z, Cheng N, Mo Y, Lu L, Hou J, Li Z, Nie X, Gao S, Hua Q (2025) Recent advances in NIR-II photothermal and photodynamic therapies for drug-resistant wound infections. *Mater Today Bio* **32**:101871
15. Semenova O, Kobzev D, Yazbak F, Nakonechny F, Kolosova O, Tatarets A, Gellerman G, Patsenker L (2021) Unexpected effect of iodine atoms in heptamethine cyanine dyes on the photodynamic eradication of Gram-positive and Gram-negative pathogens. *Dyes Pigm* **195**:109745
16. Bokan M, Nakonechny F, Talalai E, Kobzev D, Gellerman G, Patsenker L (2020) Photodynamic effect of novel hexa-iodinated quinono-cyanine dye on *Staphylococcus aureus*. *Photodiagnosis Photodyn Ther* **31**:101866
17. Kobzev D, Semenova O, Tatarets A, Bazylevich A, Gellerman G, Patsenker L (2023) Antibody-guided iodinated cyanine for near-IR photoimmunotherapy. *Dyes Pigm* **212**:111101
18. Barth BM, Altınoğlu Eİ, Shanmugavelandy SS, Kaiser JM, Crespo-Gonzalez D, DiVittore NA, McGovern C, Goff TM, Keasey NR, Adair JH, Loughran TP, Claxton DF, Kester M (2011) Targeted indocyanine-green-loaded calcium phosphosilicate nanoparticles for in vivo photodynamic therapy of leukemia. *ACS Nano* **5**:5325–5337
19. Kobzev D, Kulyk O, Semenova O, Ananieva V, Zhikol O, Omelchenko I, Tatarets A (2025) Unravelling the intricacies of fluorescence enhancement in heptamethine cyanine dyes induced by heavy halogen atoms. *Dyes Pigm* **234**:112548
20. Xiao X, Zhao X, Chen X, Zhao J (2023) Heavy Atom-Free Triplet Photosensitizers: Molecular Structure Design, Photophysical Properties and Application in Photodynamic Therapy. *Molecules* **28**:2170
21. Nguyen VN, Liang H, Jeong H, Bang J, Koh CW, Swamy KMK, Park S, Park J, Yu F, Yoon J (2026) Molecular Design of Highly Efficient Heavy-Atom-Free Near-Infrared Cyanine Photosensitizers for Fluorescence Image-Guided Photodynamic Therapy of Solid Tumors. *Adv Healthc Mater* **15**:e05692
22. Alkilany AM, Murphy CJ (2010) Toxicity and cellular uptake of gold nanoparticles: what have we learned so far? *J Nanopart Res* **12**:2313–2333
23. Murphy CJ, Gole AM, Stone JW, Sisco PN, Alkilany AM, Goldsmith EC, Baxter SC (2008) Gold nanoparticles in biology: beyond toxicity to cellular imaging. *Acc Chem Res* **41**:1721–1730
24. Chen H, Shao L, Li Q, Wang J (2013) Gold nanorods and their plasmonic properties. *Chem Soc Rev* **42**:2679–2724
25. Huang X, Neretina S, El-Sayed MA (2009) Gold nanorods: From synthesis and properties to biological and biomedical applications. *Adv Mater* **21**:4880–4910
26. Huang X, El-Sayed IH, Qian W, El-Sayed MA (2006) Cancer cell imaging and photothermal therapy in the near-infrared region by using gold nanorods. *J Am Chem Soc* **128**:2115–2120
27. Tam F, Goodrich GP, Johnson BR, Halas NJ (2007) Plasmonic enhancement of molecular fluorescence. *Nano Lett* **7**:496–501
28. Novotny L, van Hulst N (2011) Antennas for light. *Nat Photonics* **5**:83–90
29. Darvill D, Suhail A, Zhang J (2013) Plasmonic fluorescence enhancement by metal nanostructures: shaping the future of bionanotechnology. *Phys Chem Chem Phys* **15**:15709–15726

30. Aslan K, Gryczynski I, Malicka J, Matveeva E, Lakowicz JR, Geddes CD (2005) Metal-enhanced fluorescence: an emerging tool in biotechnology. *Curr Opin Biotechnol* **16**:55–62
31. Geddes CD, Lakowicz JR (2002) Metal-enhanced fluorescence. *J Fluoresc* **12**:121–129
32. Pniakowska A, Olesiak-Banska J (2022) Plasmonic enhancement of two-photon excited luminescence of gold nanoclusters. *Molecules* **27**:807
33. Zhao T, Yu K, Li J, Zhang C, Zhang Z, Zhang H (2014) Gold nanorod-enhanced singlet oxygen generation of photosensitizers. *J Phys Chem C* **118**:13200–13207
34. Luck KA, Halas NJ (2020) Near-infrared photosensitizers and plasmonic nanostructures for enhanced photodynamic therapy. *Acc Chem Res* **53**:2618–2628
35. Gunaydin G, Gedik ME, Ayan S (2021) Photodynamic therapy – current limitations and novel approaches. *Front Chem* **9**:691697
36. Niidome T, Yamamuro M, Yamaguchi A, Takahashi H, Niidome Y (2006) PEG-modified gold nanorods with high biocompatibility. *J Control Release* **114**:343–347
37. Sperling RA, Parak WJ (2010) Surface modification, functionalization and bioconjugation of colloidal inorganic nanoparticles. *Philos Trans R Soc A* **368**:1333–1383
38. Li S, Shen X, Xu QH, Cao Y (2019) Gold nanorod enhanced conjugated polymer/photosensitizer composite nanoparticles for simultaneous two-photon excitation fluorescence imaging and photodynamic therapy. *Nanoscale* **11**:19551–19560
39. Zhao C, Liu H, Huang S, Guo Y, Xu L (2024) Metal–organic framework-capped gold nanorod hybrids for combinatorial cancer therapy. *Molecules* **29**:2384
40. Kutsevol N, Bezuglyi M, Bezugla T, Rawiso M (2014) Star-Like Dextran-graft-(polyacrylamide-co-polyacrylic acid) Copolymers. *Macromol Symp* **335**:12–16
41. Jans H, Jans K, Lagae L, Borghs G, Maes G, Huo Q (2010) Poly(acrylic acid)-stabilized colloidal gold nanoparticles: synthesis and properties. *Nanotechnology* **21**:455702
42. Chumachenko V, Virych P, Nie G, Virych P, Yeshchenko O, Khort P, Tkachenko A, Prokopiuk V, Lukianova N, Zadvornyi T, Rawiso M, Ding L, Kutsevol N (2023) Combined Dextran-Graft-Polyacrylamide/Zinc Oxide Nanocarrier for Effective Anticancer Therapy in vitro. *Int J Nanomedicine* **18**:4821–4838
43. Grebinyk A, Prylutska S, Grebinyk S, Ponomarenko S, Virych P, Chumachenko V, Kutsevol N, Prylutskyy Y, Ritter U, Frohme M (2022) Drug delivery with a pH-sensitive star-like dextran-graft polyacrylamide copolymer. *Nanoscale Adv* **4**:5077–5088
44. Tkachenko A, Virych P, Myasoyedov V, Prokopiuk V, Onishchenko A, Butov D, Kuziv Y, Yeshchenko O, Zhong S, Nie G, Kutsevol N (2022) Cytotoxicity of Hybrid Noble Metal-Polymer Composites. *BioMed Res Int* **2022**:1487024
45. Kutsevol N, Bezugla T, Bezuglyi M, Rawiso M (2012) Branched Dextran-graft-Polyacrylamide Copolymers as Perspective Materials for Nanotechnology. *Macromol Symp* **317–318**:82–90
46. Yeshchenko O, Khort P, Fedotov O, Chumachenko V, Virych P, Warren HS, Booth BW, Bliznyuk V, Kutsevol N (2024) Third-generation anticancer photodynamic therapy systems based on star-like anionic polyacrylamide polymer, gold nanoparticles, and temoporfin photosensitizer. *Molecules* **29**:2224
47. Yeshchenko OA, Kutsevol NV, Tomchuk AV, Khort PS, Virych PA, Chumachenko VA, Kuziv YI, Naumenko AP, Marinin AI (2022) Plasmonic enhancement of the antibacterial photodynamic efficiency of a zinc tetraphenylporphyrin photosensitizer/dextran graft polyacrylamide anionic copolymer/Au nanoparticles hybrid nanosystem. *RSC Adv* **12**:6390–6400
48. Yeshchenko O, Kutsevol N, Virych P, Khort P, Virych P, Chumachenko V, Cekhun V (2024) Anti-cancer activity of zinc-tetraphenylporphyrin photosensitizer/dextran-graft-polyacrylamide copolymer/Au(Ag) nanoparticle nanohybrids. *RSC Adv* **14**:5045–5054

49. Nikoobakht B, El-Sayed MA (2003) Preparation and Growth Mechanism of Gold Nanorods (NRs) Using Seed-Mediated Growth Method. *Chem Mater* **15**:1957–1962
50. Atta S, Zhao Y, Li JQ, Vo-Dinh T (2024) Dual-Modal Colorimetric and Surface-Enhanced Raman Scattering (SERS)-Based Lateral Flow Immunoassay for Ultrasensitive Detection of SARS-CoV-2 Using a Plasmonic Gold Nanocrown. *Anal Chem* **96**:4783–4790
51. Klimov V (2014) Nanoplasmonics. Jenny Stanford Publishing, Singapore
52. Maier SA (2007) Plasmonics: Fundamentals and Applications. Springer, New York
53. Dolinnyi AI (2015) Nanometric rulers based on plasmon coupling in pairs of gold nanoparticles. *J Phys Chem C* **119**:4990–5001
54. Su Q, Jiang C, Gou D, Long Y (2021) Surface plasmon-assisted fluorescence enhancing and quenching: From theory to application. *ACS Appl Bio Mater* **4**:4684–4705
55. Medintz I, Hildebrandt N (eds) (2013) FRET – Förster Resonance Energy Transfer: From Theory to Applications. Wiley-VCH, Weinheim
56. Boyd GT, Rasing T, Leite JRR, Shen YR (1984) Local-field enhancement on rough surfaces of metals, semimetals, and semiconductors with the use of optical second-harmonic generation. *Phys Rev B* **30**:519–526
57. Johnson PB, Christy RW (1972) Optical constants of the noble metals. *Phys Rev B* **6**:4370–4379